Soils and Rocks
An International Journal of Geotechnical and Geoenvironmental Engineering
www.soilsandrocks.com
ISSN 1980-9743
ISSN-e 2675-5475

Influence of soft soil properties on the performance of unreinforced embankments: a finite element study

Laura Zappellini Sassi[1#], Naloan Coutinho Sampa[1]

Article

Keywords
Soft soil
Numerical analysis
Parametric analysis
Unreinforced embankment

Abstract

This study investigates the behavior of four unreinforced embankments on soft soils through numerical and parametric analyses. The embankments, composed of granular material, are 3.5 m in height and 17 m in width, and are modeled over a clay layer extending 30 m horizontally, with thicknesses of 5, 10, 15, and 20 m. The soft soil was simulated with the modified Cam Clay model, and the embankment fill with the Mohr–Coulomb criterion. Forty Abaqus simulations were performed, varying soil thickness, overconsolidation ratio (OCR), recompression index (κ), and critical state line slope (M). The analyses evaluated settlement, horizontal displacement, pore pressure, effective vertical stress and mobilized soil volume, applying multiple normalization approaches. Results highlight the strong influence of soil thickness and κ on deformation and pore pressure, the limited effect of M and OCR for thicker layers and confirm the usefulness of mobilized volume criteria for stability evaluation.

1. Introduction

Embankment construction on soft soils remains a key academic and practical concern due to urbanization, infrastructure demands, and land reclamation in densely populated areas. These projects involve low-strength and compressible soils, requiring a mix of construction techniques, design strategies, and monitoring systems to ensure stability, predict settlements, and assess performance during and after construction.

Numerous studies have investigated the stability and settlement behavior of embankments on soft soils. Predictive methods typically assess embankment performance based on stability, as well as on the evolution of settlement, lateral displacement, and pore pressure over time (Brugger, 1996; Massad, 2021). Settlement is traditionally estimated using Terzaghi's (1925) one-dimensional consolidation theory, later extended by Terzaghi & Fröhlich (1936). This theory describes consolidation as the time-dependent volume reduction of saturated soil caused by the dissipation of excess pore water pressure under self-weight or external loading (DNER, 2022) and relates variation in excess of pore pressure to effective stress and void ratio (Budhu, 2010).

According to the effective stress principle, embankment construction induces excess pore pressure in the soft soil, thereby modifying effective stress. Evaluating pore pressure and effective stress supports the control of embankment elevation rates and enhances the interpretation of soil strength and safety factors over time (Coutinho, 1986; Ortigão, 1980). Depending on soil properties and elevation rate, consolidation may begin during construction, as pore pressure dissipates and strength progressively increases.

Several researchers have studied the performance of instrumented embankments through the analysis of volumetric, horizontal and vertical displacements. Tavenas et al. (1979) investigated the relationship between the maximum horizontal displacement ($\delta_{h,max}$) and settlement ($\rho_{máx}$), noting that values of $\delta_{h,máx} / \rho_{max}$ between 0.09 and 0.27 correspond to approximately elastic behavior in overconsolidated clays, while ratios between 0.71 and 1.31 reflect the elastoplastic behavior of normally consolidated clays. Ratios consistently in the range of 0.14 to 0.18 were associated with the consolidation phase. Loganathan et al. (1993) proposed the Field Deformation Analysis (FDA) method, introducing parameters that describe vertical and horizontal displacement relationships.

Sandroni et al. (2004) proposed an empirical method to assess stability based on the ratio between horizontal and vertical volumes (V_v / V_h) and its rate of change (dV_v / dV_h) over time (t) and embankment height (H). During loading, values above 3 indicate stability, while values near 1 suggest failure. In the consolidation phase, under constant loading and undrained conditions, values exceeding 5 denote stability, whereas lower values warrant caution.

#Corresponding author. E-mail address: lazasassi@gmail.com
[1]Universidade Federal de Santa Catarina, Departamento de Engenharia Civil, Florianópolis, SC, Brasil.

Submitted on August 15, 2025; Final Acceptance on December 2, 2025; Discussion open until August 31, 2026.
Editor: Renato P. Cunha
https://doi.org/10.28927/SR.2026.013425

Finite element methods (FEM) have become increasingly prominent in evaluating the stability, settlement, and performance of embankments on soft soils, especially for complex geometries or parametric studies. They have been widely used to complement limit equilibrium methods by predicting deformation, stress, pore pressures, and safety factors (DNER, 2022).

To further the understanding of embankment behavior and address existing gaps in numerical modeling, this study presents numerical and parametric simulations conducted in Abaqus, investigating the influence of OCR, κ, M, and H_s on settlement, horizontal displacement, pore pressure, effective stress and mobilized volume of four unreinforced embankments.

2. Methods

Numerical analyses were performed in Abaqus under plane strain conditions, using four symmetric two-dimensional models of unreinforced embankments. Abaqus was selected due to its robust implementation of the modified Cam Clay model, its capability for fully coupled pore pressure-deformation analysis, and its flexibility in defining complex boundary and loading conditions under plane strain. Each model consisted of a granular embankment with a height of 3.5 m and a base width of 17 m, constructed over a homogeneous soft clay layer with thicknesses of 5 to 20 m, and a horizontal extension of 30 m. To reduce computational cost, only half of the domain (Figure 1) was modeled, exploiting its symmetry.

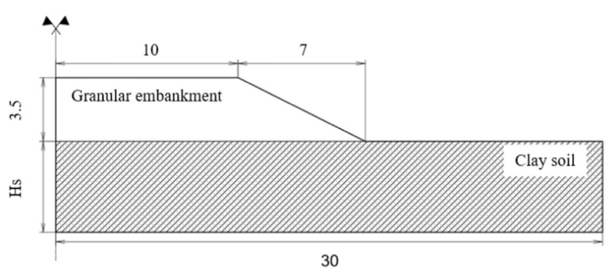

Figure 1. Half-domain of the numerical model, in m.

2.1 Geotechnical parameters

The embankment fill was modeled as a dry, homogeneous material using the Mohr-Coulomb failure criterion. The clay layer was represented as a homogeneous elastoplastic material governed by the modified Cam Clay model. Table 1 presents the parameters adopted for both materials, based on typical values for soft clays in Florianópolis, as reported by Oliveira (2006) and Baran (2014).

2.2 Simulation steps

The simulations followed a three-step procedure, representing embankment construction in a single stage. The first step established the initial geostatic stresses by applying gravity loading using the “body force” function. In the second step, the embankment was constructed incrementally up to a height of 3.5 m over one month. The third step simulated the consolidation of the clay layer over a period of 48 months. Throughout all stages, the evolution of settlement, mobilized soil volume, horizontal displacement, excess pore pressure, and effective stress were monitored.

2.3 Boundary conditions and finite element mesh

The model employed physical and hydraulic boundary conditions representative of field conditions under plane strain assumptions. Vertically and horizontally fixed boundary conditions were applied at the model base, while horizontal displacements were restrained on the lateral edges. Pore pressure at the ground surface was set to zero throughout the simulation to represent free drainage.

Table 1. Geotechnical parameters of the soft soil and granular material.

Granular material		Clay	
Parameter	Value	Parameter	Value
Initial void ratio - e_0	0.65	Initial void ratio - e_0	2.5
Bulk unit weight - γ (kN/m³)	20	Bulk unit weight - γ (kN/m³)	15
Cohesion - c (kN/m²)	2	Recompression index - κ	0.065
Internal friccional angle - ϕ (º)	30	Poisson's ratio - ν	0.33
Dilatancy angle - ψ (º)	0	Compression index - λ	0.65
Elastic Module - E (kN/m²)	1000	Slope of the critical state line - M	1
Poisson's ratio - ν	0.3	Overconsolidation ratio - OCR	0.75, 1.0, 1.5, 3.0
Permeability coefficient - k (m/s)	0.01	Size of the yield surface in the wet side - β	1
		Ratio of the flow stress - K	1
		Permeability coefficient - k (m/s)	2.50E-08
		Lateral earth pressure at rest – $K_0 = 1 - \text{sen}\phi$	0.57

The embankment was discretized with CPE8R elements, and the foundation with CPE8RP elements. Figure 2 shows the mesh configuration and boundary conditions for the model with a 5 m thick soil. The mesh was refined in regions expected to experience high stress and deformation gradients.

2.4 Parametric analyses

To assess the influence of soil parameters on embankment performance, 10 parametric analyses were conducted for each of the four models, totaling 40 simulations. Parameters varied included M, κ, OCR, and H_s.

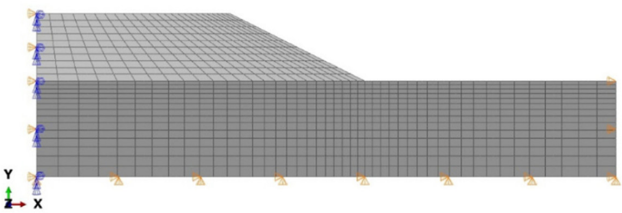

Figure 2. Boundary conditions and finite element mesh for model with H_s = 5 m.

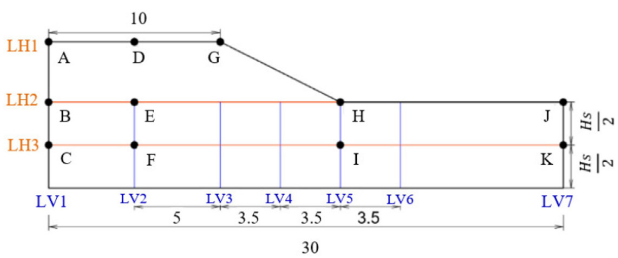

Figure 3. Location of observation points and lines, in m.

Table 2 presents the values used in each parametric analysis. Analysis 1 was the reference case with standard values, while the remaining analyses altered only one parameter at a time, keeping the others constant. No changes were made to the embankment filling properties. Except for OCR = 0.75, all parameter values are consistent with typical ranges reported for Florianópolis clays (Oliveira, 2006; Baran, 2014). The OCR of 0.75 was considered to investigate the response of clay undergoing consolidation, rather than for practical application.

Results were exported from Abaqus to Microsoft Excel for graphical representation and interpretation. To support the analysis, 11 observation points (A to K), three horizontal lines (LH1 to LH3), and six vertical lines (LV1 to LV6) were defined within the model to examine temporal and spatial variation of key response variables. Figure 3 shows the locations of these points and lines within the model domain.

3. Results

This section presents the results of the 40 numerical simulations, focusing on the effects of soft soil H_s, OCR, κ, and M on settlement, horizontal displacement, excess pore pressure, effective stress and mobilized soil volume. Due to space limitations, only representative results and figures are included; however, the discussion encompasses trends observed across all analyses.

3.1 Settlement

Figure 4 illustrates the spatial distribution of settlement for the reference model (H_s = 5 m) at the end of embankment construction (1 month) and after the consolidation phase (48 months). Areas of greater settlement are shown in blue, while positive values indicate upward ground movement.

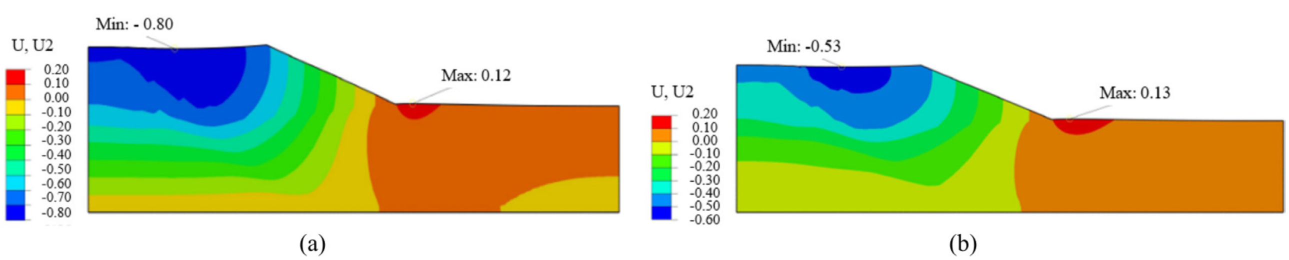

Figure 4. Spatial distribution of settlement: (a) 1 month and (b) 48 months.

Table 2. Parameters and values used in parametric analyses.

Analysis	M	Analysis	κ	Analysis	OCR
1 (reference)	1.0	1 (reference)	0.065	1 (reference)	1.00
2	1.1	5	0.050	8	0.75
3	1.2	6	0.080	9	1.50
4	1.3	7	0.095	10	3.00

Downward displacements occur beneath the embankment crest, while upward movements near the embankment toe may result from lateral soil displacement.

Normalized settlement (ρ / H_s) was evaluated over the square root of time ($\sqrt{t}$) at key points (A, B, D, E, G, and H), as well as along horizontal lines LH1 and LH2, at 1 month and 48 months. As expected, and shown in Figure 4, settlements within the clay layer (points C, F, I, and K and LH3) are smaller than the total layer settlements; therefore, they were not evaluated individually due to this behavior and space limitations. Effective normalized settlement $\left(\rho / H_s\right).\left(\sigma'_{vo} / q\right)$ was also assessed using the average geostatic stress and embankment surcharge along the lines LH1 and LH2 for the same periods of time.

Figure 5 presents the variation of ρ / H_s at points B and H. At point B, settlement increases nonlinearly with time until reaching stability. At point H, initial upward movement is later reversed in most cases (except in analyses with H_s = 5 m and OCR = 0.75 and 1.0), possibly resulting from consolidation effects or numerical modeling. Further investigation is required to determine the underlying cause.

Regardless of the value of H_s, increasing the κ parameter reduces ρ / H_s. The maximum value of ρ / H_s tends to occur near the toe of the embankment for $H_s \geq 10$ m. On the axis of symmetry, ρ / H_s varies between 1.91% and 3.56% for H_s of 20 m, between 2.25% and 4.22% for H_s of 15 m, between 4.39% and 7.99% for H_s of 10 m, and between 4.22% and 15.00% for H_s of 5 m.

In general, increasing H_s reduces the settlement stabilization time (T_{set}), which is below 9.5 months in all analyses. Analyses with H_s = 5 m do not show significant influence of M and κ on T_{set}. Contrarily, T_{set} decreases as OCR increase from 0.75 to 3.

Table 3 provides a summary of the percentage range of ρ / H_s. The consolidation process causes ground heave near the slope toe, followed by a marked reduction post-construction. The results confirm that thicker soil layers reduce ρ / H_s, with OCR and M having minor effects for $H_s \geq 10$ m. For H_s = 5 m, variations in κ produce more pronounced differences.

Figure 6 shows normalized curves accounting for the average geostatic stress (σ'_{v0}) and the embankment surcharge ($q = \gamma H_e = 70\text{kPa}$). The results are unaffected by H_s due to the inclusion of σ'_{v0}. The influence of M and OCR on $\left(\rho / H_s\right).\left(\sigma'_{vo} / q\right)$ is evident only for H_s = 5 m, while an increase in κ slightly reduces $\left(\rho / H_s\right).\left(\sigma'_{vo} / q\right)$ for $H_s \geq 10$ m.

3.2 Horizontal displacement

Figure 7 shows the spatial distribution of horizontal displacement, at 1 month and 48 months. The ratio δ_h / ρ is crucial for assessing slope performance, as excessive horizontal movement relative to settlement (red area) can generate shear stress zones and lead to failure.

Table 3. Percentage range of ρ / H_s for analyses with different H_s.

Parametric analysis	Percentage of ρ / H_s (1 month)	Percentage of ρ / H_s (48 months)
	$H_s = 5\,\text{m}$	
M	(5.0-5.1)	(10-10.8)
k	(4.7-6.6)	(10.2-12.8)
OCR	(4.1-6.8)	(4.2-15.0)
	$H_s = 10\,m$	
M	(4.1)	(5.5)
k	(3.3-5.5)	(4.4-8.0)
OCR	(4.1)	(5.5-7.9)
	$H_s = 15\,\text{m}$	
M	(2.3)	(2.9)
k	(1.8-3.1)	(2.3-4.2)
OCR	(2.3)	(2.9)
	$H_s = 20\,\text{m}$	
M	(1.9)	(2.5)
k	(1.5-2.6)	(1.9-3.6)
OCR	(1.9)	(2.5)

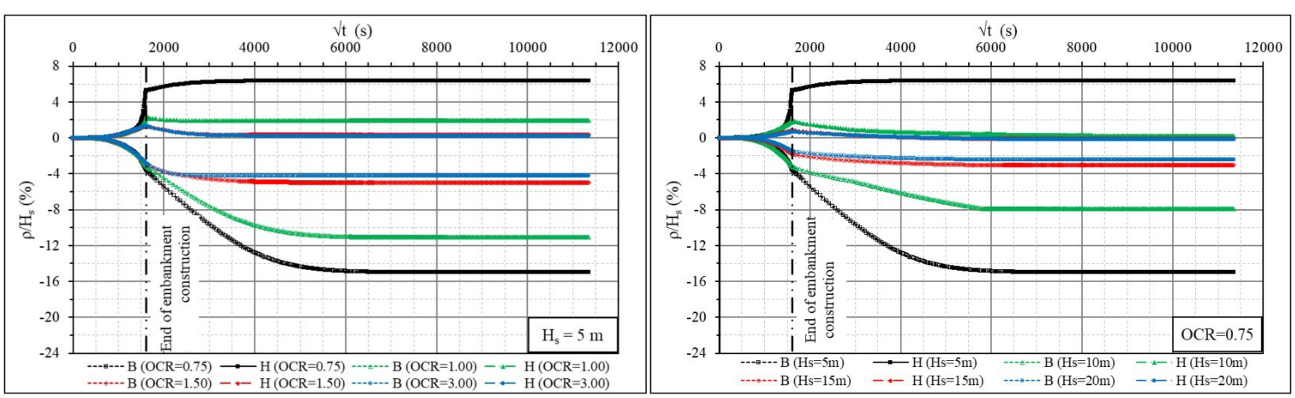

(a) (b)

Figure 5. Variation of ρ / H_s versus ($\sqrt{t}$): (a) H_s = 5 m with varying OCR and (b) OCR = 0.75 with varying H_s.

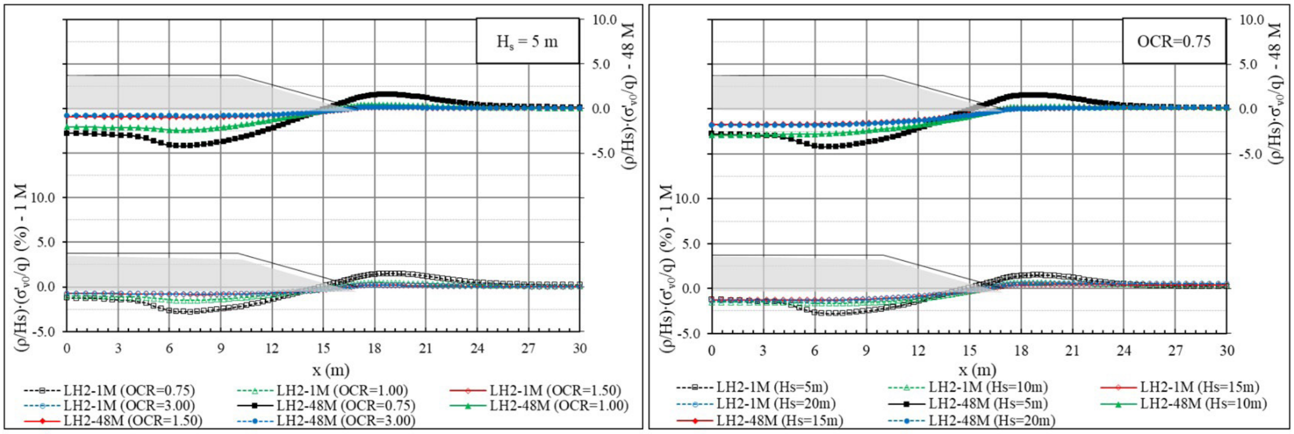

Figure 6. Variation of $(\rho / H_s).(\sigma'_{v0} / q)$ along LH2: (a) H_s = 5 m with varying OCR and (b) OCR = 0.75 with varying H_s.

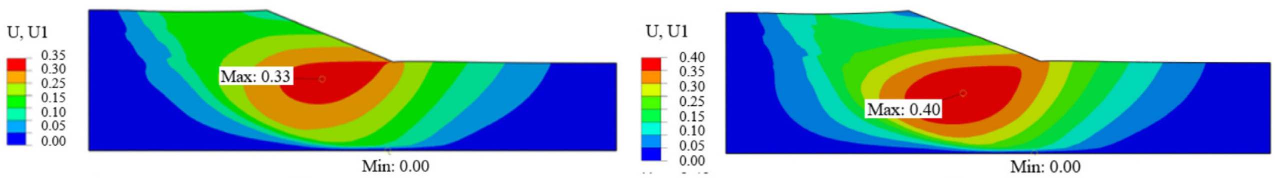

Figure 7. Spatial distribution of the horizontal displacement: (a) 1 month and (b) 48 months.

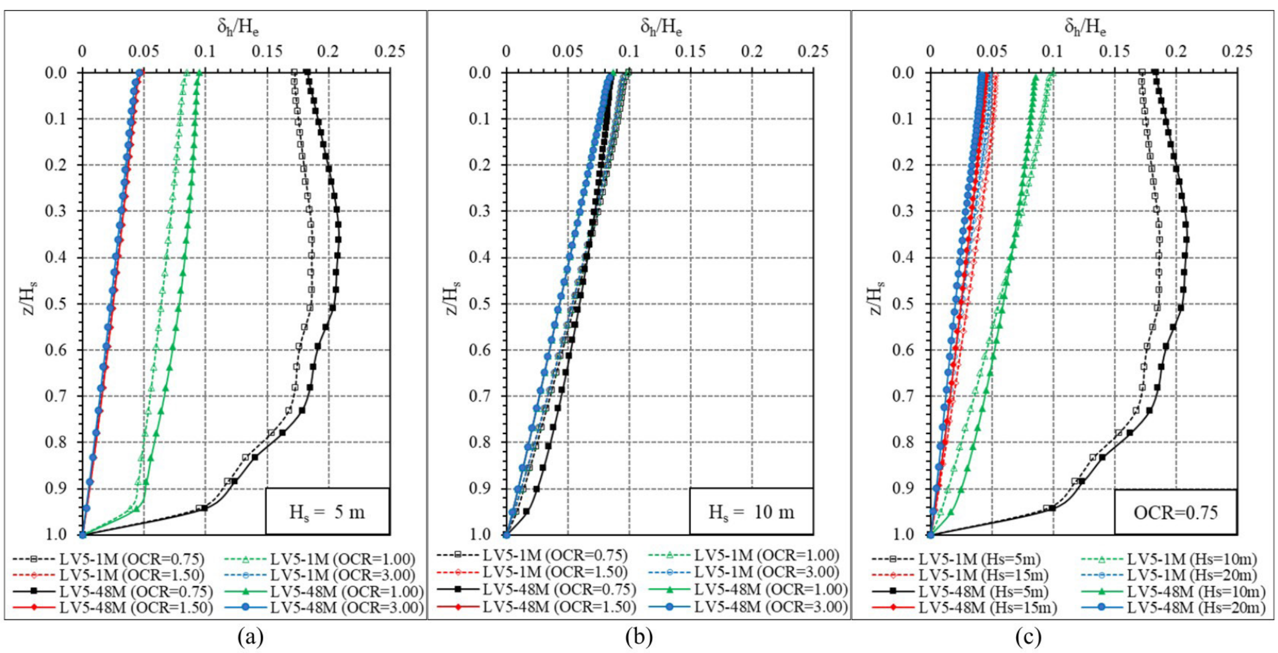

Figure 8. Variation of δ_h / H_e versus z / H_s: (a) H_s = 5 m with varying OCR, (b) H_s = 10 m with varying OCR, and (c) OCR = 0.75 with varying H_s.

Figure 8 presents the typical variation of δ_h / H_e along z / H_s for LV5 in analyses with H_s of 5 m and 10 m, varying OCR values. In models with H_s = 5 m, δ_h / H_e increases after embankment construction, as was observed by Brugger (1996). Models with H_s = 10, 15, and 20 m show the opposite trend, consistent with Loganathan et al. (1993). Further study is needed to clarify this reversal, although Brugger (1996) attributes it to limitations in numerical modeling approaches.

The $\left(\delta_h / H_e\right)_{max}$ typically occurs at the soft soil surface (z / H_s = 0), except for LV3 in some H_s = 5 m cases, where values remain nearly constant from z / H_s = 0.1 to 0.7, then drop to zero at z / H_s = 1. In most cases, the profile is curvilinear, although some display an almost linear decrease from maximum at the surface to zero at the base.

The boundary condition at z / H_s = 1 constrains horizontal displacement at the model base. Given that analyses with H_s = 20 m show δ_h / H_e extending to greater depths, it is reasonable to infer that, base values for H_s = 5, 10, and 20 m could exceed zero if unconstrained. This suggests that all tested soft soil thicknesses are inadequate in fully restraining horizontal displacement at the base.

Parametric studies showed that increasing κ raises δ_h / H_e for all H_s values. For LV5, $\left(\delta_h / H_e\right)_{max}$ ranged from 7.7 - 12.5%, 6.5 - 12.7%, 3.7 - 7.3%, and 3.1 - 6.3% for H_s = 5, 10, 15, and 20 m, respectively. Changes in M and OCR affected δ_h / H_e only for H_s = 5 m. For LV5 with H_s = 5 m, varying M yielded $\left(\delta_h / H_e\right)_{max}$ between 5.5 - 9.5%, while OCR variation gave $\left(\delta_h / H_e\right)_{max}$ between 4.6 - 21.0% for H_s = 5 m, and from 4.2% - 8.4% for H_s = 10, 15, and 20 m.

In most cases, $\left(\delta_h / H_e\right)_{max}$ was below 10%, except in the critical case with OCR = 0.75 and 5 m thick, where it reached 21%. For H_s = 10 m, changes in M and κ had little effect, while OCR variation had the greatest impact on displacement reversal, followed by M and then κ.

The $\delta_{h,max} / \rho_{max}$ at 1 month ranged from 0.318 - 0.652 (H_s = 5 m), 0.459 - 0.561 (H_s = 10 m), 0.328 - 0.409 (H_s = 15 m), and 0.275 - 0.341 (H_s = 20 m). After consolidation, these values dropped to 0.184 - 0.474, 0.234 - 0.274, 0.197 - 0.212, and 0.164 - 0.169, respectively. The $\delta_{h,max} / \rho_{max}$ decreased with increasing H_s According to Tavenas et al. (1979), $\delta_{h,max} / \rho_{max}$ between 0.09 and 0.27 indicates approximately elastic behavior, while values from 0.71 to 1.31 reflect elasto-plastic behavior.

3.3 Mobilized soil volume

The mobilized volumes above the embankment provide a more realistic assessment of embankment behavior on clays (Brugger, 1996) and allow stability to be monitored through limit ratios of vertical and horizontal volumes (Sandroni et al., 2004).

This study analyzes the vertical volumes V_{v1} and V_{v2}, and the horizontal volume $\left(V_h\right)$, using the ratios V_{v2} / V_{v1}, V_h / V_{v1} and V_h / V_{v2}. Here, V_{v1} is the vertical volume mobilized beneath the embankment, V_{v2} is the vertical volume mobilized near the toe, and V_h is the horizontal volume mobilized along line LV5.

Figure 9 shows the effect of parameters on V_{v1} and V_{v2} / V_{v1}. Variations in M and OCR have no effect on V_{v1} or V_{v2} / V_{v1} for $H_s \geq 10$ m. The V_{v2} / V_{v1} is unaffected by κ after consolidation but is slightly influenced by κ immediately after embankment construction. In contrast, V_{v1} increases with higher κ. The ranges of V_{v1} and V_{v2} / V_{v1} for each H_s. are summarized in Table 4.

Figure 10 shows the effect of pameter variations on V_h / V_{v1} and V_h / V_{v2}. Both δ_h and V_h decrease with distance from the slope crest, with V_h highest for LV3, followed by LV5 and LV6.

The trend in V_h mirrors that of δ_h. For H_s = 5 m, V_h increases after embankment construction; for H_s = 10, 15, and 20 m, it decreases during consolidation. For H_s = 10 m, both V_h and V_{v1} slightly decrease with increasing H_s and remain relatively stable with variations in M, κ, and OCR. In contrast, for H_s = 5 m, V_h and V_{v1} decrease with higher M and OCR and increase with higher κ.

The ranges of V_h / V_{v1} and V_h / V_{v2} for each H_s at 1 month and 48 months are presented in Table 5. The V_h / V_{v1} results indicate stable conditions, with values below 0.33 (or $V_{v1} / V_h > 3$) at 1 month and below 0.20 (or $V_{v1} / V_h > 5$) at 48 months, in agreement with the stability limits proposed by Sandroni et al. (2004).

Table 4. The range of V_{v1} and V_{v1} / V_{v2} for analyses with different H_s.

Parametric analysis	Range of V_{v1}							
	$H_s = 5$ m		$H_s = 10$ m		$H_s = 15$ m		$H_s = 20$ m	
	1M	48M	1M	48M	1M	48M	1M	48M
M	3.8-5.2	6.3-8.9	8.9	8.8-8.9	7.8	7.1	9.0	7.9
k	4.4-6.5	7.1-9.4	6.9-12.7	6.9-12.7	6.0-11.1	5.5-10.3	7.0-12.9	6.1-11.4
OCR	3.3-8.7	3.3-13.0	8.8-9.0	8.8-11.3	7.8	7.1-7.3	9.0	7.9
Parametric analysis	Range of V_{v1} / V_{v2}							
	$H_s = 5$ m		$H_s = 10$ m		$H_s = 15$ m		$H_s = 20$ m	
	1M	48M	1M	48M	1M	48M	1M	48M
M	0.11-0.18	0.04-0.10	0.21	0.06	0.20	0.06	0.21	0.04
k	0.17-0.20	0.09-0.10	0.19-0.30	0.06	0.19-0.22	0.06	0.20-0.22	0.04
OCR	0.05-0.21	0.10-0.33	0.21	0.06-0.07	0.20	0.06	0.21	0.04

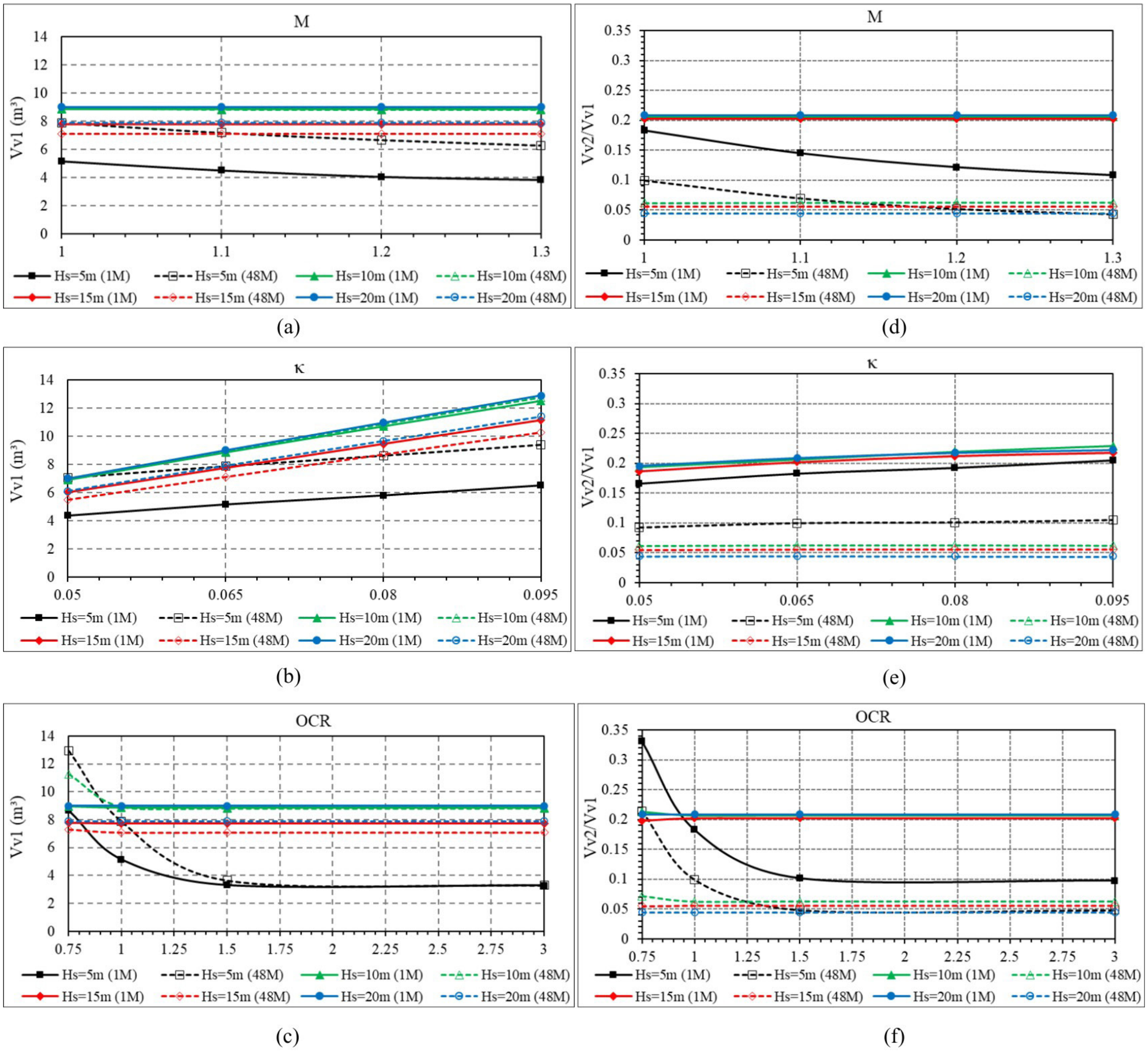

Figure 9. Influence of the parameters κ, M and OCR on V_{v1} and V_{v2} / V_{v1}: (a) M versus V_{v1} (m³), (b) κ versus V_{v1} (m³), (c) OCR versus V_{v1} (m³), (d) M versus V_{v2} / V_{v1}, (e) κ versus V_{v2} / V_{v1}, and (f) OCR versus V_{v2} / V_{v1}.

3.4 Excess pore pressure and effective vertical stress

Figure 11 shows the spatial distribution of excess pore pressure. Red regions indicate maximum values. After 1 month, the peak excess pore pressure was 32.16 kPa near the base at the axis of symmetry. By 48 months, the excess pore pressure had almost dissipated, approaching zero.

Excess pore pressure was normalized by the embankment surcharge at the soft soil surface ($q = \gamma_a H_a = 70\,\text{kPa}$) and analyzed along LV1, LV2, and LV5. Four additional normalization methods were applied along LH3.

Figure 12 shows normalized pore pressure $(\Delta u / q)$ versus normalized depth $(\Delta u / q)$ and illustrates the influence of κ and H_s on $(\Delta u / q)$ along lines LV1, LV5, and LV2. $(\Delta u / q)$ values are highest along LV1.

In all lines, $(\Delta u / q)$ increases with depth. The variation of $(\Delta u / q)$ along LV1 and LV5 display similar trends, differing from LV2. On LV1 and LV5, values rise nearly linearly at shallow depths before stabilizing; LV2 shows a nonlinear increase before leveling off. At shallow depths, LV2 values are generally lower than LV5; at greater depths, the opposite occurs.

Increasing H_s shifts the z / H_s where $(\Delta u / q)$ values along LV2 and LV5 converge. For M-variation analyses, z / H_s rises from 0.55 to 0.79 as H_s increases from 5 to

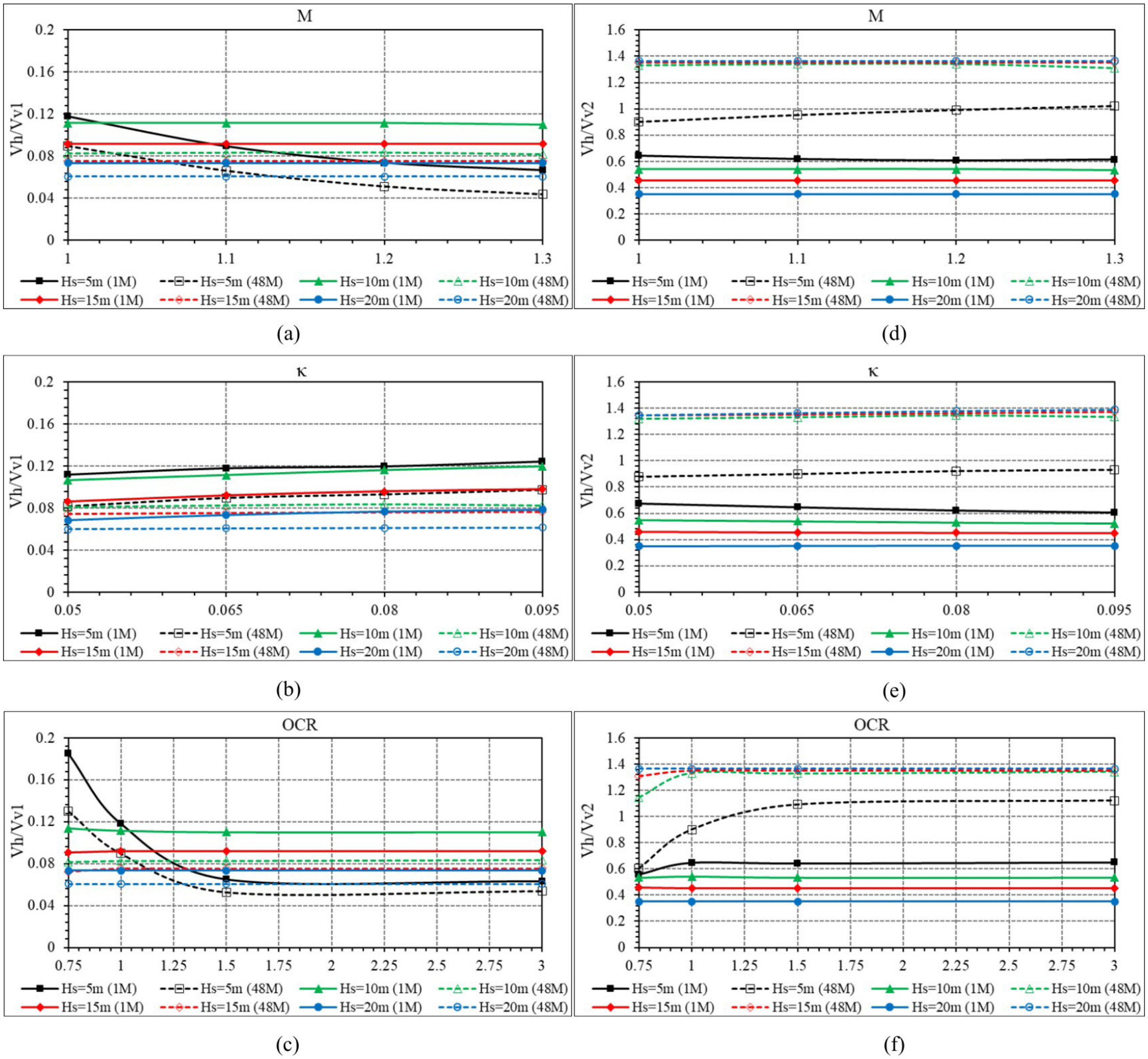

Figure 10. Influence of the parameters κ,M and OCR on V_h / V_{v1} and V_h / V_{v2}: (a) M versus V_h / V_{v1} (m³), (b) κ versus V_h / V_{v1} (m³), (c) OCR versus V_h / V_{v1} (m³), (d) M versus V_h / V_{v2}, (e) κ versus V_h / V_{v2}, and (f) OCR versus V_h / V_{v2}.

20 m. For κ variation, it rises from 0.45 to 0.84; for OCR variation, from 0.60 to 0.78.

For a given z / H_s and vertical line, $(\Delta u / q)$ increases with H_s, due to longer drainage paths. κ has the largest influence: higher κ yields higher $(\Delta u / q)$, with stronger effects for larger H_s. M has negligible influence on $(\Delta u / q)$ for any H_s, and OCR affects $(\Delta u / q)$ only for H_s = 5 m, where higher OCR reduces $(\Delta u / q)$.

Figure 13 presents four different normalization methods of pore pressure. First $\Delta u / \sigma'_v$, excess pore pressure divided by the effective vertical stress after embankment construction. Second $\Delta u / \sigma'_{v0}$, excess pore pressure divided by the initial effective vertical stress. Third $\Delta u / \Delta\sigma'_v$, excess pore pressure divided by the change in effective vertical stress during construction. Fourth $U = 1 - \Delta u / q$, degree of consolidation.

For $\Delta u / \sigma'_v$ (Figure 13a), pore pressure decreases more slowly beneath the embankment than outside it. $\Delta u / \sigma'_v$ values drop from maximum at the axis of symmetry to minimum at the right boundary. $\Delta u / \sigma'_{v0}$ (Figure 13b) shows a faster decrease along LH3. Most results of $\Delta u / \sigma'_v$ are below 0.84, but some exceed 1 for H_s = 5 m and for H_s = 20 m

Table 5. The range of V_h / V_{v1} and V_h / V_{v2} for analyses with different H_s.

Parametric analysis	Range of V_h / V_{v1}							
	$H_s = 5\,m$		$H_s = 10\,m$		$H_s = 15\,m$		$H_s = 20\,m$	
	1M	48M	1M	48M	1M	48M	1M	48M
M	0.07-0.12	0.04-0.09	0.11	0.08	0.09	0.08	0.07	0.06
k	0.11-0.12	0.08-0.1	0.11-0.12	0.08	0.09-0.1	0.07-0.08	0.07-0.08	0.06
OCR	0.06-0.18	0.05-0.13	0.11	0.08	0.09	0.07-0.08	0.07	0.06
Parametric analysis	Range of V_h / V_{v2}							
	$H_s = 5\,m$		$H_s = 10\,m$		$H_s = 15\,m$		$H_s = 20\,m$	
	1M	48M	1M	48M	1M	48M	1M	48M
M	0.61-0.65	0.9-1.02	0.53-0.54	1.31-1.33	0.45	1.35	0.35	1.36
k	0.61-0.67	0.88-0.93	0.52-0.55	1.32-1.35	0.45-0.46	1.34-1.37	0.35	1.36-1.39
OCR	0.56-0.65	0.61-1.12	0.53-0.54	1.15-1.34	0.45-0.46	1.31-1.35	0.35	1.36

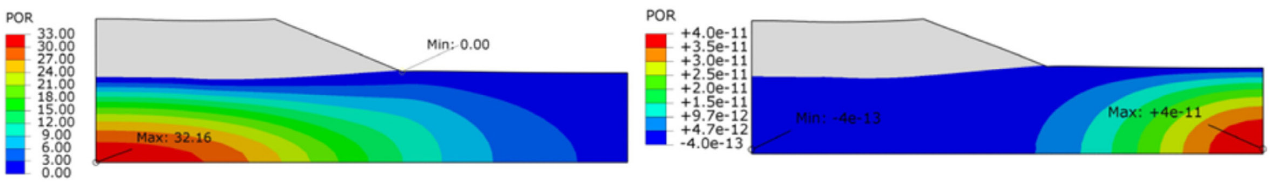

(a) (b)

Figure 11. Spatial distribution of excess pore pressure: (a) 1 month and (b) 48 months.

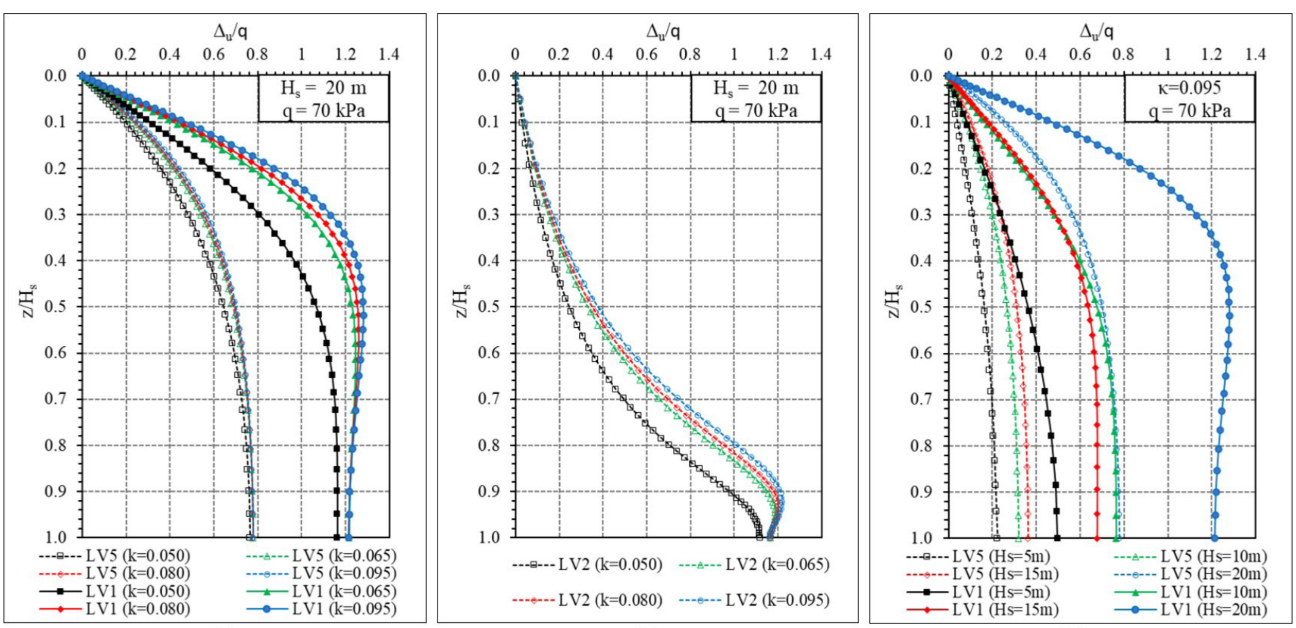

(a) (b) (c)

Figure 12. Variation of $\Delta u / q$ versus z / H_s: (a) LV5 and LVI lines, H_s = 20 m with varying κ, (b) LV2, H_s = 20 m with varying κ, and (c) LV5 and LVI lines, κ = 0.095 with varying H_s.

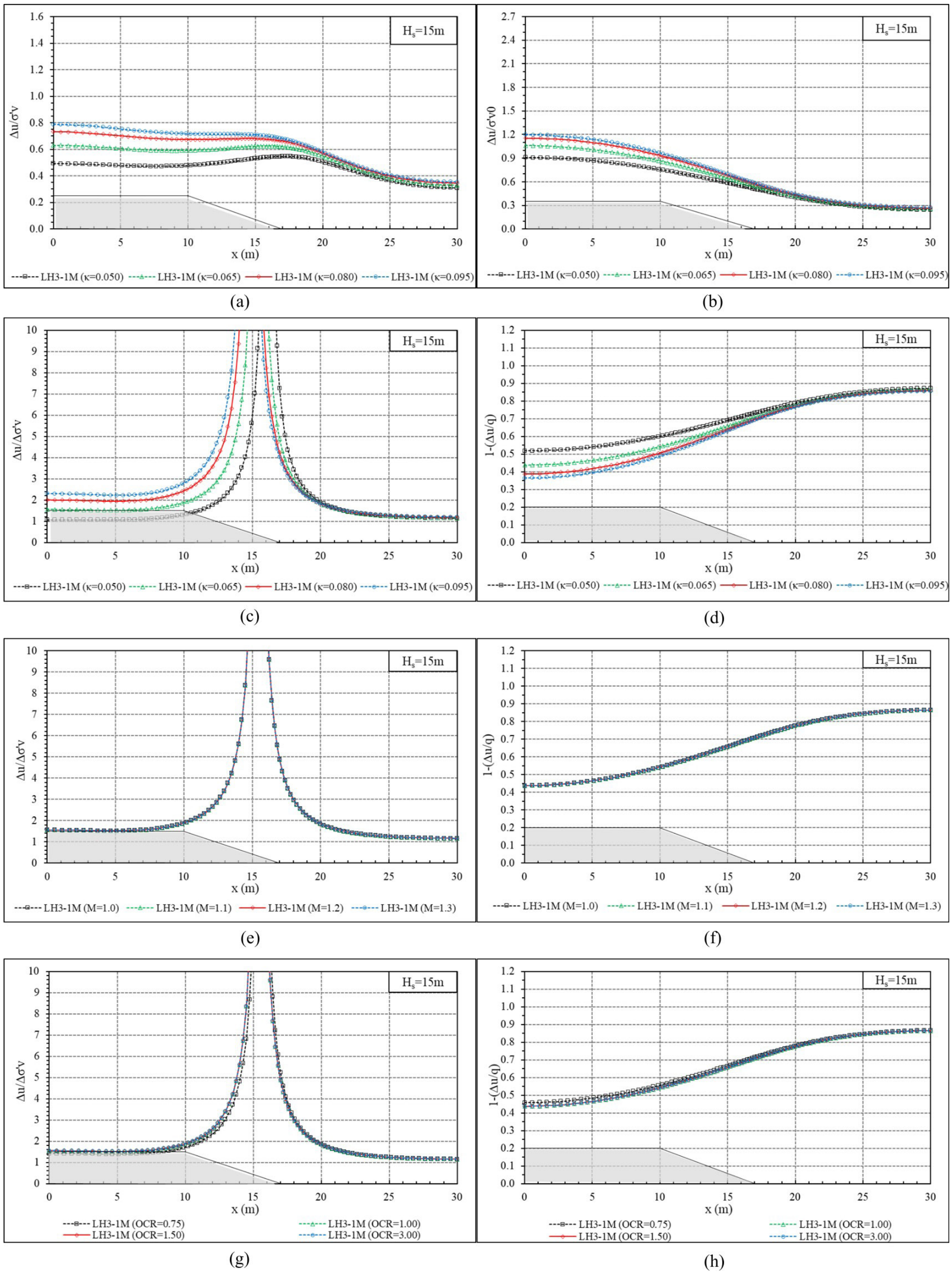

Figure 13. Variation of normalized excess pore pressure and degree of consolidation along LH3: (a) $\Delta u / \sigma'_v$ for H_s = 15 m with varying κ, (b) $\Delta u / \sigma'_{v0}$ for H_s = 15 m with varying κ, (c) $\Delta u / \Delta\sigma'_v$ for H_s = 15 m with varying κ, (d) $(1 - \Delta u / q)$ for H_s = 15 m with varying κ, (e) $\Delta u / \Delta\sigma'_v$ for H_s = 15 m with varying M, (f) $(1 - \Delta u / q)$ for H_s = 15 m with varying M, (g) $\Delta u / \Delta\sigma'_v$. for H_s = 15 m with varying OCR, and (h) $(1 - \Delta u / q)$ for H_s = 15 m with varying OCR.

with OCR = 0.080 - 0.095. For $H_s \geq 10$ m, $\Delta u / \sigma'_v$ and $\Delta u / \sigma'_{v0}$ nerally decrease with increasing H_s. M and OCR have minimal influence except at H_s = 5 m, where higher values reduce $\Delta u / \sigma'_v$. Higher κ increases $\Delta u / \sigma'_v$ but decreases $\Delta u / \sigma'_{v0}$ beneath the embankment. In this region, $\Delta u / \sigma'_{v0}$ tends to exceed 1, particularly for H_s = 5 and 10 m.

High $\Delta u / \Delta\sigma'_v$ indicates low consolidation and possible instability under the slope. $\Delta u / \Delta\sigma'_v$ values (Figure 13c, Figure 13e, Figure 13g) increase with H_s, especially beneath the embankment. M and OCR have little influence on $\Delta u / \Delta\sigma'_v$, and M, OCR, and κ changes have no impact on $\Delta u / \Delta\sigma'_v$ in the unloaded soil near the right boundary. Higher κ increases $\Delta u / \Delta\sigma'_v$ beneath the embankment. Along LH3, two patterns of $\Delta u / \Delta\sigma'_v$ emerge: constant values below 3 under the crest and outside the embankment; and peaks above 10 beneath the slope, suggesting shear zone formation and potential instability.

During consolidation, excess pore pressure dissipation corresponds to increased effective stress. Beneath the crest, the increase in effective stress can be up to three times greater than during construction; beneath the slope, it can exceed ten times.

For degree of consolidation (U), M and OCR have minimal influence. U increases as H_s decreases, particularly near the right boundary. Along LH3, U rises from 0.35 - 0.45 near the symmetry axis to 0.8 - 1.0 at the right boundary. Values near 1 indicate complete dissipation of excess pore pressure.

4. Conclusion

This study evaluated the combined influence of soft soil H_s, OCR, κ, and M on the performance of unreinforced embankments through forty finite element simulations. The results demonstrate that embankment behavior results from the interaction among these parameters, with H_s exerting primary control and the others modulating its effects.

H_s governs both deformation and drainage mechanisms. Increasing H_s reduces ρ / H_s, δ_h / H_e, and excess pore pressure, producing faster stabilization for the same embankment height. Thin layers (H_s = 5 m) show more complex displacement patterns, such as upward movement at the toe followed by reversal. In these cases, OCR, κ, and M interactions become more evident, jointly influencing stiffness recovery, volumetric change, and shear redistribution.

The OCR and κ interaction plays a central role in defining time-dependent compressibility and consolidation. Higher κ increases settlement and excess pore pressure ($\Delta u / q$), while higher OCR enhances stiffness and accelerates consolidation. Their combined effect governs both the rate and the magnitude of settlement stabilization. Low OCR with high κ yields slower consolidation and higher $\Delta u / \sigma'_v$, whereas high OCR with low κ promotes faster stress redistribution and lower settlements.

The parameter M affects the stress-strain path and the extent of plastic zones. Although compared with H_s, OCR, and κ, M influences horizontal deformation trends and displacement reversal in thinner layers, but has negligible impact for $H_s \geq 10$ m.

Interdependence among H_s, OCR, and κ is also reflected in the mobilized soil volumes. Higher κ increases both vertical and horizontal mobilized volumes (V_{v1} and V_h), while higher OCR reduces them, producing more stable configurations. The ratios V_{v2} / V_{v1} and V_h / V_{v1} remain within the stability limits proposed by Sandroni et al. (2004), confirming the adequacy of the mobilized volume approach to capture coupled deformation and drainage mechanisms.

Although the assumption of a homogeneous clay layer limits direct generalization to stratified profiles, the normalized response patterns derived here provide valuable guidance for preliminary assessments. They clarify the mechanical coupling among OCR, κ, M, and H_s, establish consistent behavioral trends, and support the interpretation and prediction of embankment performance on soft clays in early design stages prior to detailed site-specific modeling.

Acknowledgements

The authors would like to express gratitude for the support provided by the Federal University of Santa Catarina (UFSC) and the National Council for Scientific and Technological Development (CNPq).

Declaration of interest

The authors have no conflicts of interest to declare. All co-authors have observed and affirmed the contents of the paper and there is no financial interest to report.

Authors' contributions

Laura Zappellini Sassi: data curation, visualization, writing – original draft. Naloan Coutinho Sampa: conceptualization, methodology, supervision, validation, writing – review & editing, funding acquisition.

Data availability

The datasets generated analyzed in the course of the current study are available from the corresponding author upon request.

Declaration of use of generative artificial intelligence

This work was prepared with the assistance of generative artificial intelligence (GenAI) Copilot, to support the translation of the text. The entire process of using this tool was supervised, reviewed and when necessary edited by the authors. The authors assume full responsibility for the content of the publication that involved the aid of GenAI.

List of symbols and abbreviations

c	Cohesion
e_0	Initial void ratio
k	Permeability coefficient
q	Embankment surcharge
t	Time
x	Horizontal distance
z	Depth
E	Elastic Module
H_e	Embankment height
H_s	Thickness of the soft soil
K	Ratio of the flow stress
K_0	Lateral earth pressure at rest
M	Slope of the critical state line
OCR	Overconsolidation ratio
T_{set}	Stabilization time of the settlement
U	Degree of consolidation
V_h	Horizontal volume
V_v	Vertical volume
V_{v1}	Vertical volume mobilized below the embankment
V_{v2}	Vertical volume mobilized near the toe of the embankment
β	Size of the yield surface in the wet side
γ	Bulk unit weight
δ_h	Horizontal displacement
$\delta_{h,máx}$	Maximum horizontal displacement
κ	Recompression index
λ	Compression index
ν	Poisson's ratio
ρ	Settlement
$\rho_{máx}$	Maximum settlement
ϕ	Internal frictional angle
ψ	Dilatancy angle
Δu	Variation in excess pore pressure
$\Delta\sigma'_v$	Variation in effective vertical stress
σ'_v	Effective vertical stress
σ'_{v0}	Average geostatic stress

References

Baran, K. (2014). *Propriedades geotécnicas de compressibilidade de uma argila mole de Itajaí, SC* [Master's dissertation]. Federal University of Santa Catarina (in Portuguese).

Brugger, P.J. (1996). *Análise de deformações em aterros sobre solos moles* [Doctoral thesis]. Federal University of Rio de Janeiro (in Portuguese). Retrieved in August 15, 2025, from https://minerva.ufrj.br/F/?func=direct&doc_number=000207020&local_base=UFR01

Budhu, M. (2010). *Soil mechanics and foundations* (3rd ed.). Chichester: John Wiley & Sons.

Coutinho, R.Q. (1986). *Aterro experimental instrumentado levado à ruptura sobre solos orgânicos-argilas moles da barragem de Juturnaíba* [Doctoral thesis]. Federal University of Rio de Janeiro (in Portuguese).

DNER PRO 381/98. (2022). *Projeto de aterros sobre solos moles para obras viárias.* Departamento Nacional de Estradas de Rodagem, Rio de Janeiro.

Loganathan, N., Balasubramaniam, A.S., & Bergado, D.T. (1993). Deformation analysis of embankments. *Journal of Geotechnical Engineering*, 119(8), 1185-1206.

Massad, F. (2021). *Obras de terra: curso básico de geotecnia* (2. ed.). São Paulo: Oficina de Textos.

Oliveira, H.M. (2006). *Comportamento de aterros reforçados sobre solos moles levados à ruptura* [Doctoral thesis]. Federal University of Rio de Janeiro (in Portuguese). Retrieved in August 15, 2025, from https://portal.coc.ufrj.br/en/teses-de-doutorado/150-2006/1071-henrique-magnani-de-oliveira

Ortigão, J.A.R. (1980). *Aterro experimental levado à ruptura sobre argila cinza do Rio de Janeiro* [Doctoral thesis]. Federal University of Rio de Janeiro (in Portuguese).

Sandroni, S.S., Lacerda, W.A., & Brandt, J.R.T. (2004). Método dos volumes para controle de campo da estabilidade de aterros sobre argilas moles. *Soils and Rocks*, 27(1), 25-35.

Tavenas, F., Mieussens, C., & Bourges, F. (1979). Lateral displacements in clay foundations under embankments. *Canadian Geotechnical Journal*, 16(3), 532-550.

Terzaghi, K. (1925). *Erdbaumechanik*. Vienna: Franz Deuticke (in German).

Terzaghi, K., & Fröhlich, O.K. (1936). *Thoerie der Setzung von Tonschichten*. Leipzig: Franz Deuticke (in German).